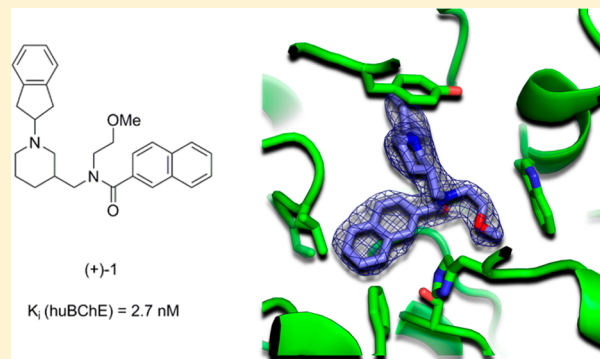


Discovery, Biological Evaluation, and Crystal Structure of a Novel Nanomolar Selective Butyrylcholinesterase Inhibitor

Boris Brus,[†] Urban Košak,[†] Samo Turk,^{†,▽} Anja Pišlar,[†] Nicolas Coquelle,^{‡,§,||} Janko Kos,^{†,⊥} Jure Stojan,[#] Jacques-Philippe Colletier,^{*,‡,§,||} and Stanislav Gobec^{*,†}[†]Faculty of Pharmacy, University of Ljubljana, Aškerčeva 7, 1000 Ljubljana, Slovenia[‡]IBS, University Grenoble Alpes, F-38044 Grenoble, France[§]IBS, CNRS, F-38044 Grenoble, France^{||}IBS, CEA, F-38044 Grenoble, France[⊥]Jožef Stefan Institute, Jamova 39, 1000 Ljubljana, Slovenia[#]Institute of Biochemistry, Faculty of Medicine, University of Ljubljana, Vrazov trg 2, 1000 Ljubljana, Slovenia

Supporting Information

ABSTRACT: Butyrylcholinesterase (BChE) is regarded as a promising drug target as its levels and activity significantly increase in the late stages of Alzheimer's disease. To discover novel BChE inhibitors, we used a hierarchical virtual screening protocol followed by biochemical evaluation of 40 highest scoring hit compounds. Three of the compounds identified showed significant inhibitory activities against BChE. The most potent, compound **1** ($IC_{50} = 21.3$ nM), was resynthesized and resolved into its pure enantiomers. A high degree of stereoselective activity was revealed, and a dissociation constant of 2.7 nM was determined for the most potent stereoisomer (+)-**1**. The crystal structure of human BChE in complex with compound (+)-**1** was solved, revealing the binding mode and providing clues for potential optimization. Additionally, compound **1** inhibited amyloid β_{1-42} peptide self-induced aggregation into fibrils (by 61.7% at 10 μ M) and protected cultured SH-SY5Y cells against amyloid- β -induced toxicity. These data suggest that compound **1** represents a promising candidate for hit-to-lead follow-up in the drug-discovery process against Alzheimer's disease.



INTRODUCTION

Alzheimer's disease (AD) is a debilitating and fatal progressive neurodegenerative disorder that has a devastating impact on humans. Worldwide, it is estimated that 35 million people suffer from dementia, with most cases due to AD.¹ Although the etiology of AD is not yet entirely known, several conditions are believed to have important roles in the pathogenesis of this disease such as aggregation and accumulation of amyloid- β ($A\beta$) deposits,^{2,3} oxidative stress,⁴ and low levels of neurotransmitter acetylcholine (ACh).⁵

According to the cholinergic hypothesis for AD pathogenesis, the decline of hippocampal and cortical levels of ACh leads to dysfunction of the cholinergic system and results in severe memory and learning deficits.⁶ At the neuronal level, ACh can be degraded by two types of cholinesterases (ChEs): acetylcholinesterase (AChE) and butyrylcholinesterase (BChE). AChE activity is dominant in the healthy brain (80%), where BChE seems to play only a supportive role. Accordingly, AChE is mainly expressed by neurons, while BChE activity is mainly associated with glial cells.⁷ Over the past decade, several anti-AD drugs targeting AChE have been launched on the market, including donepezil,^{8,9} rivastigmine,¹⁰

and the alkaloid galanthamine.¹¹ The characterization of an AChE nullizygote mouse demonstrated, however, that BChE can rescue the cholinesteratic function in the absence of AChE.¹² This finding is in agreement with earlier reports that showed an inversion of AChE and BChE relative expressions during AD progression. Furthermore, BChE knockout mice show no physiological disadvantage, and silent BChE mutations in humans show a slower rate of cognitive decline.^{13,14} Hence, it is expected that inhibiting BChE could benefit AD patients the same way AChE inhibition does. In vivo data supporting this hypothesis include the observation that specific BChE inhibitors are able to restore ACh levels in mice¹⁵ and improve the cognitive performance of mice treated with the amyloid- β peptide,^{16–18} yet without peripheral (parasympathomimetic) adverse side effects,^{15,16} which are known to limit the dosing of AChE inhibitors.^{19–21} Therefore, several selective BChE inhibitors have been described, the most potent of which are the carbamate analogues of cymserine²² and isosorbide,²³ which (pseudo)irreversibly inhibit the enzyme (Figure 1). The

Received: August 4, 2014

Published: September 16, 2014

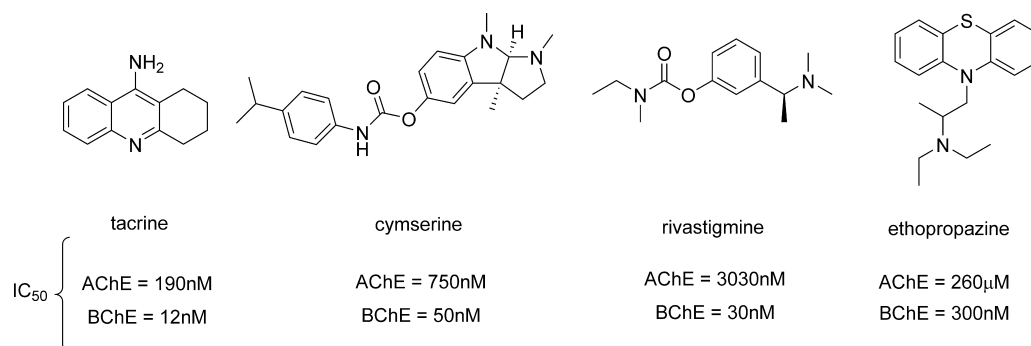


Figure 1. Cholinesterase inhibitors with various degree of selectivity for BChE.

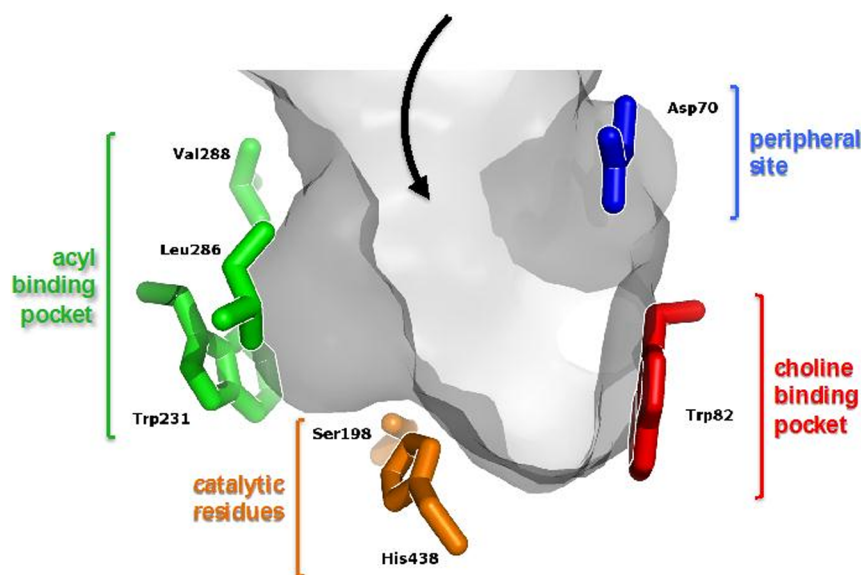


Figure 2. Schematic representation of the active site gorge of human BChE. The principal contributors the peripheral anionic site (Asp 70; blue), the choline-binding pocket (Trp82; red), and the acyl-binding pocket (Trp231, Leu286, and Val288; green) are shown in sticks, as well as the catalytic serine and histidine (Ser198 and His438; orange). The black arrow indicates the route taken by substrates and ligands to enter the gorge.

tacrine-based dual ChE inhibitors have also gained a lot of attention despite tacrine being withdrawn from the market due to the hepatotoxicity of its metabolites.^{24–27}

AChE and BChE share 65% amino acid sequence homology.^{28–30} They display a similar overall structure, and their active sites, composed of a catalytic triad and an choline binding pocket, are both buried at the bottom of a ~20 Å deep gorge. The two enzymes differ by the presence and extent of subdomains within the gorge, including a midgorge aromatic recognition site, a peripheral anionic site, and an acyl-binding pocket (Figure 2). The most remarkable difference concerns the acyl-binding pocket, which accommodates the acyl moiety of the substrate during catalysis. AChE residues Phe288 and Phe290 are replaced by Leu286 and Val288 in BChE, allowing the latter to both bind and hydrolyze bulkier ligands and substrates. Accordingly, BChE is known to act as a natural scavenger in the bloodstream.^{31,32} To the best of our knowledge, no structure-based virtual screening methods have been applied in the BChE hit-discovery process despite the availability of a high resolution crystal structure.^{28,33} However, studies employing various docking algorithms were used for binding mode analysis of known BChE inhibitors.^{34–36}

In the present study, we report on the successful application of a hierarchical structure-based virtual screening which led to

the discovery of three novel and selective reversible inhibitors of huBChE. The complex structure of huBChE with the most potent of these, compound 1, was solved, revealing the molecular basis for its action. Additionally, the antiamyloidogenic properties of compound 1 were explored by using a thioflavin T-based fluorometric assay, and studies on neuroblastoma SH-SY5Y cells further demonstrated its neuroprotective effects against A β neurotoxicity.

RESULTS AND DISCUSSION

Virtual Screening. In recent years, structure-based virtual screening has become routine in both pharmaceutical companies and academic groups as a complementary method to high-throughput screening for the early stage hit discovery process.^{37–40} Despite the ever-increasing processing power of modern computers, blind docking with entire compound databases often leads to wasted time and computational resources. It is also well accepted that the content and quality of a compound database are crucial for the success of any virtual screening.^{41,42} To strike a balance between speed, efficiency, and quality, hierarchical filtering was performed using OBGREP and FILTER software. ChEs are characterized by a deeply buried active site gorge, lined with aromatic residues, and feature acidic residues at both the entrance

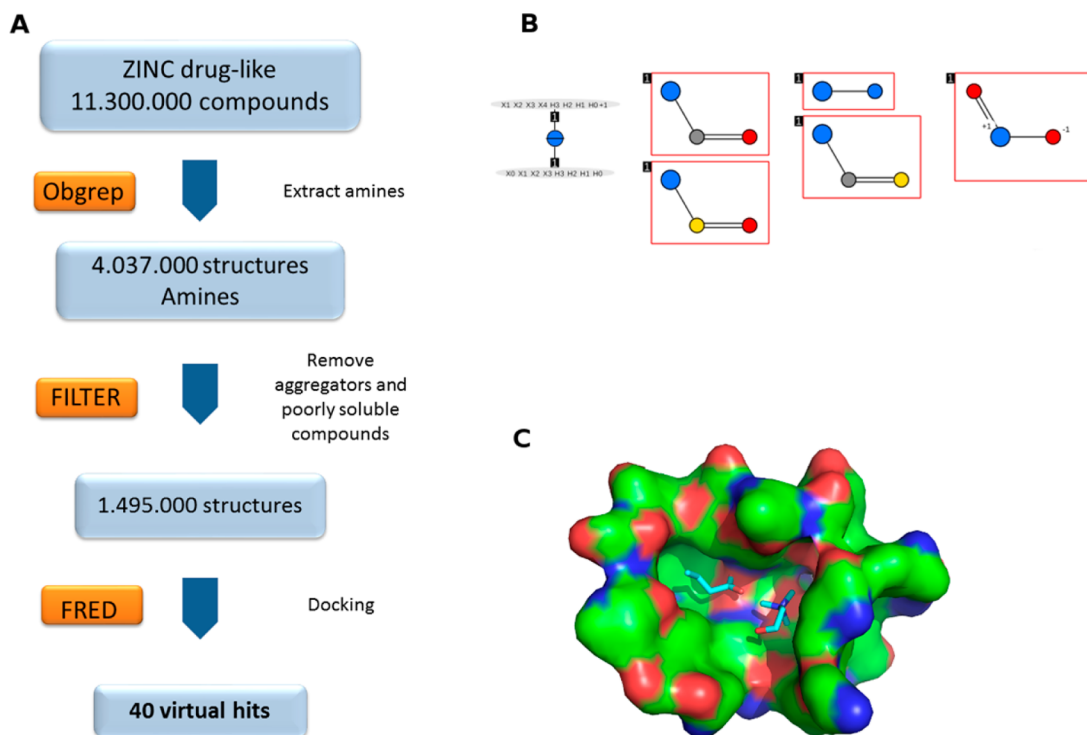


Figure 3. (A) Flowchart summarizing the hierarchical structure-based virtual screening. (B) Visualization of the molecular pattern in form of a SMARTS, as used for the amine search inside the ZINC drug-like database. The structures in red rectangles are not hits. The visualization was prepared using SMARTSViewer.⁵⁰ (C) The active site pocket of huBChE (PDB code 1P0M) with the aligned butanoic acid (PDB code 1P0I) used for docking of the filtered database.

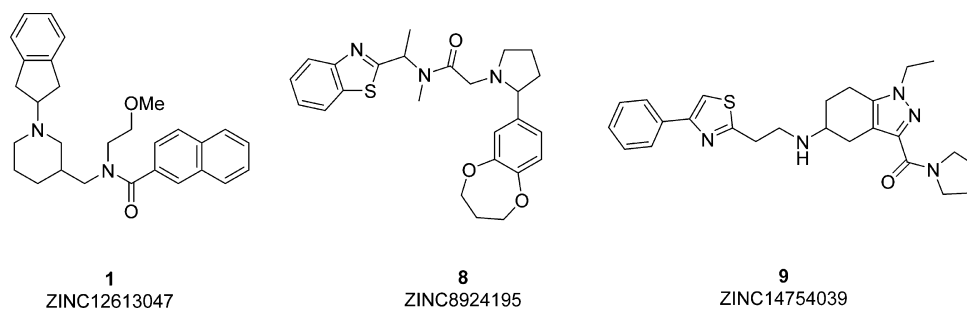


Figure 4. Structures of the novel huBChE inhibitors obtained through the hierarchical docking protocol. Compounds 1 and 9 were obtained as mixtures of enantiomers and compound 8 as a mixture of diastereomers.

(Asp70 in huBChE) and the bottom of the gorge (Glu197 in huBChE). The latter effect in generating a strong electrostatic potential that attracts positively charged substrates and inhibitors into and down the gorge.^{43,44} Additionally, crystallographic studies have revealed that positively charged ligands can also interact with aromatic residues in ChEs active site gorge via cation- π interactions.^{28,45,46} Thus, basic or permanently charged nitrogens are common amidst ChE ligands (Figure 1). Accordingly, we used OBGREP software to subselect compounds bearing an amine moiety, while FILTER software was used to remove insoluble and aggregating compounds. Thereby, the ZINC drug-like subset of 11.3 million compounds was narrowed down to a focused database of roughly 1.5 million compounds (see Compound Database Preparation in the Experimental Section for details).^{47,48}

Structure-based virtual screening was then performed using as a model the crystal structure of huBChE in complex with a choline molecule (PDB code 1P0M) and FRED docking software (Figure 3C). FRED was proven to be by far the fastest

docking tool and thus particularly suitable for ultrahigh-throughput docking (>1 million compounds).⁴⁹ Custom constraints were implemented in the screening protocol based on the detailed analysis of the active site gorge and on the known binding modes of various substrates and inhibitors. The compounds from the focused database were then docked into the customized active site (see Molecular Docking in the Experimental Section for details). Poses of the docked compounds that satisfied the custom constraints (at least one heavy atom in contact with Ser198 and one with Trp82) were ranked according to the Chemgauss3 score (Figure 3A). The 40 top-ranked and commercially available compounds were purchased from different suppliers (compounds S1-S40, Supporting Information) and subsequently evaluated in the biochemical experiments.

Inhibition of Human BChE and Murine AChE. The 40 top hits from virtual screening were evaluated *in vitro* for their inhibition of recombinant huBChE, using the method of Ellman.⁵¹ Inhibitory activity was detected for seven of the 40

compounds, and among these, three compounds showed >50% inhibition at 10 μM (compounds **1**, **8**, and **9**; Figure 4). Further characterization of the inhibition properties revealed that (\pm)-*N*-((1-(2,3-dihydro-1*H*-inden-2-yl)piperidin-3-yl)methyl)-*N*-(2-methoxyethyl)-2-naphthamide ((\pm)-**1**) is the most potent huBChE inhibitor, with an IC_{50} of 21.3 nM (Figure 4, Table 1).

Table 1. Activities of the Novel BChE Inhibitors

compd no.	$\text{IC}_{50} \pm \text{SEM}$ (μM) huBChE	IC_{50} or %RA at 10 $\mu\text{M} \pm \text{SEM}$ (μM) mAChE	selectivity ^a	inhibition of $A\beta_{1-42}$ self-induced aggregation at 10 μM (%)
(\pm)- 1	0.021 ± 0.002	102.1 ± 2.5	4790	61.7 ± 3.6
8	1.36 ± 0.08	$94.0 \pm 9.6\%$	>140	ni
9	2.15 ± 0.09	ni	>110	ni
(+)- 1	0.013 ± 0.002	101.2 ± 1.5	8480	60.3 ± 7.8
(-)- 1	0.166 ± 0.005	110.3 ± 2.1	660	57.5 ± 6.2
tacrine	0.012 ± 0.003	0.106 ± 10	8.6	nd

^a IC_{50} mAChE/ IC_{50} huBChE. For compounds **8** and **9**, selectivity was calculated assuming an IC_{50} of 200 μM on mAChE due to solubility problems.

The three active hits were further assayed against mAChE, allowing evidence of their high degree of selectivity for huBChE (Table 1). Because of the poor solubility of compounds **8** and **9**, the IC_{50} against mAChE could only be determined for (\pm)-**1**, revealing >4700-fold selectivity for huBChE over mAChE (102.1 μM). The IC_{50} values of the hit compounds for ChE inhibition are given in Table 1. The dose–response curves are shown in the Supporting Information, Figure S1. Molecular docking studies were performed to reveal the rationale for the low AChE inhibitory potency by the hit compounds **1**, **8**, and **9** (Supporting Information, Figure S7).

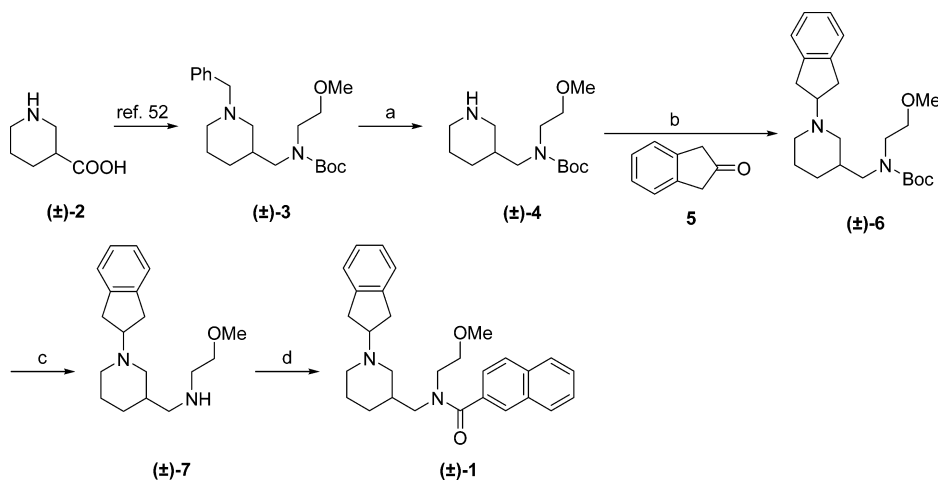
Synthesis and Chiral HPLC Resolution of the Racemic Mixture of Compound 1. Despite being commercially available, methods for the preparation of compound **1** and its potential applications have not yet been reported. For this reason, synthetic route to the racemic **1** was developed as presented in Scheme 1. Orthogonally protected piperidin-3-

ylmethanamine (\pm)-**3** was prepared from commercially available nipecotic acid [(\pm)-**2**], as previously reported.⁵² Debenzylation of *N*-benzylamine (\pm)-**3** was achieved with cyclohexene in the presence of a catalytic amount of Pearlman's catalyst (palladium hydroxide on carbon) in methanol under reflux⁵³ to provide the secondary amine (\pm)-**4**. Oxidation of 2-indanol using pyridinium chlorochromate/silica gel in dichloromethane⁵⁴ provided ketone **5**, which was reacted with crude secondary amine (\pm)-**4** in the presence of sodium triacetoxyborohydride [$\text{NaBH}(\text{OAc})_3$] and acetic acid in 1,2-dichloroethane⁵⁵ to produce the tertiary amine (\pm)-**6**. TFA in dichloromethane was used to remove the *tert*-butyloxycarbonyl protecting group from compound (\pm)-**6** to provide amine (\pm)-**7** after alkaline treatment. Then 2-naphthoic acid was treated with crude amine (\pm)-**7** in the presence of TBTU and triethylamine in dichloromethane at room temperature⁵⁶ to produce amide (\pm)-**1**.

As the preparation of the diastereoisomeric salts failed, the enantiomeric resolution of (\pm)-**1** was carried out using chiral HPLC. Several analytical conditions were checked, and aqueous sodium borate buffer (20 mM, pH 9.00) containing 49% MeCN provided almost baseline separation of these two enantiomers (Supporting Information, Figure S2). The analytical method was scaled-up for preparative separation of 60 mg of (\pm)-**1** to provide the pure enantiomers. The first-eluted enantiomer (–)-**1** gave an ee of 100%, whereas the ee of the second-eluted enantiomer (+)-**1** was 98%. The specific rotation of the first-eluted enantiomer was $[\alpha]_{\text{D}}^{23} -23.82$ (*c* 0.250, CHCl_3), while the specific rotation of the second-eluted enantiomer was $[\alpha]_{\text{D}}^{23} +24.52$ (*c* 0.260, CHCl_3).

Kinetic Evaluation of Compound 1. Stereoselectivity of BChE toward reversible inhibitors, such as ethopropazine, has already been reported.⁵⁷ In this manner, compound **1** was resolved into its pure enantiomers, (+)-**1** and (–)-**1**, which were evaluated individually. More than a 10-fold difference in the huBChE inhibitory potencies was observed, favoring the (+)-**1** enantiomer. The IC_{50} of the eutomer was 13.4 nM, which is comparable to the activity of the positive control tacrine, while the less active enantiomer had an IC_{50} of 166 nM. Enantiomers (+)-**1** and (–)-**1** retained weak potencies toward

Scheme 1. ^a



^aReagents and conditions: (a) cyclohexene, $\text{Pd}(\text{OH})_2/\text{C}$ cat., MeOH, rt to reflux, under argon, 17 h (97% crude); (b) $\text{NaBH}(\text{OAc})_3$, AcOH, 1,2-dichloroethane, rt, under argon, 72 h (83%); (c) (i) TFA, CH_2Cl_2 , rt, 22 h, (ii) 1 M aq NaOH, 0 °C (84% crude); (d) 2-naphthoic acid, TBTU, Et_3N , CH_2Cl_2 , rt, 19 h (36%).

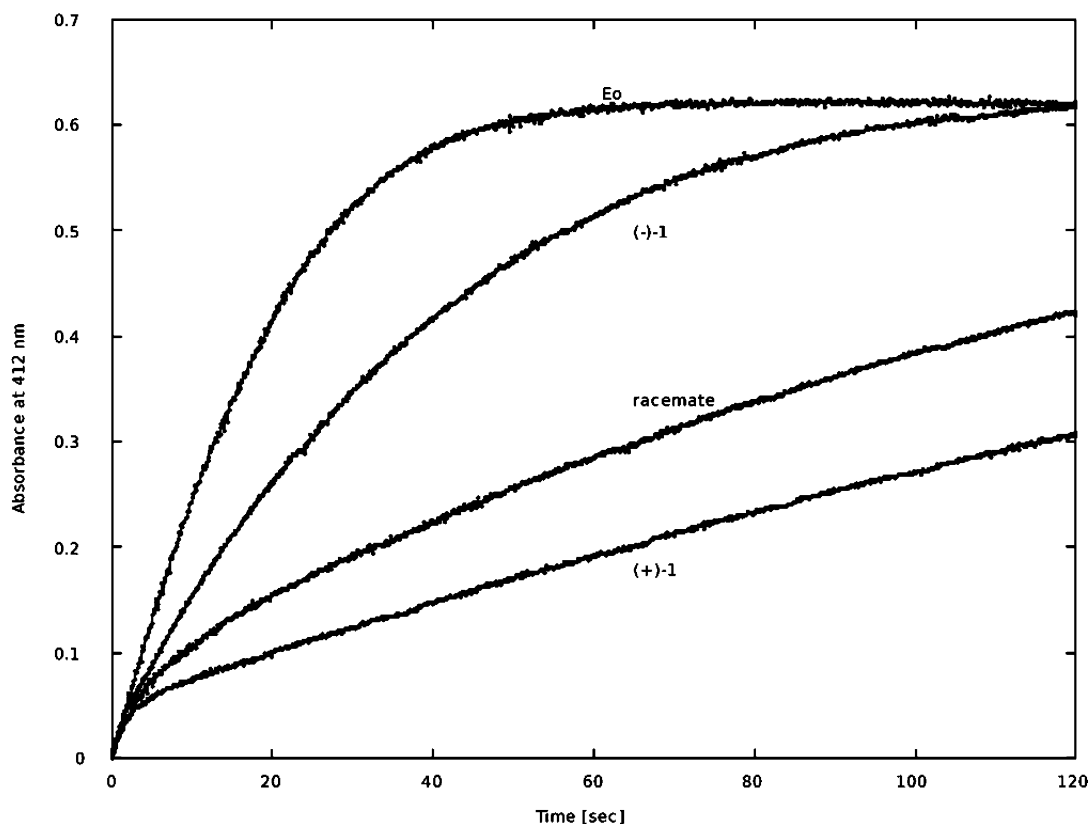
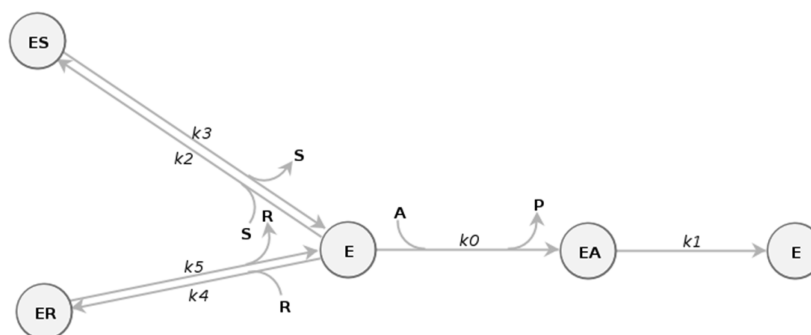


Figure 5. Progress curves for hydrolysis of BTC by huBChE in the absence (E_0) and presence of 50 nM racemic solution or each enantiomer of compound **1** obtained using the stopped-flow apparatus.

Scheme 2. Reaction Scheme of BTC Hydrolysis by huBChE in the Absence and Presence of Compound **1**^a, as Constructed by ENZO Web Tool (project no. 140429302)^a



^a(A) Substrate; (P) product; E (enzyme); (S) (-)-**1**; (R) (+)-**1**.

mAChE (IC_{50} of 101.2 and 110.3 μ M, respectively). The IC_{50} values are given in Table 1.

To obtain more detailed information about the mechanism of huBChE inhibition, kinetic experiments were performed using a stopped-flow apparatus. The progress curves obtained in the absence and presence of compound **1** (for the racemic mixture and for each individual enantiomer) are shown in Figure 5. The form of the progress curves and the concentrations of the test compound (50 nM) and huBChE (4.2 nM) used in the assay are typical for slow, tight-binding inhibition by compound **1**. This type of inhibition was further confirmed by the upward concave progress curve obtained after dilution of the enzyme preincubated with compound (\pm)-**1** (Supporting Information, Figure S3). Additionally, the identical courses of the initial portions of the curves in the absence and

presence of compound **1** clearly expose the so-called mechanism A⁵⁸ (see Scheme 2). The potential clinical advantage of the tight binding inhibition of compound **1** arise from its high affinity (low value of K_i), and the long residence time on the huBChE, due to the slow dissociation rate (low value of k_{off}).⁵⁹

The determined rates and the calculated dissociation constants for each of the enantiomers, along with the K_m and k_{cat} values for the BTC, are listed in Table 2. The results of the ENZO fit are furthermore accessible online: <http://enzo.cmm.ki.si/kinetic.php?uwd=140429302load=true>. Of note, the X-ray structure of the complex of huBChE with compound (+)-**1** (see below) demonstrates that its high affinity results from a tight accommodation into the enzyme active site. The slow action of

Table 2. Characteristic Constants for the Hydrolysis of BTC by huBChE and Its Inhibition by Compound 1 at pH 8

constant	BTC	(+)-1	(-)-1
K_m (μM)	38.4 ± 0.3		
k_{cat} (s^{-1})	852 ± 8		
k_{on} ($\text{M}^{-1} \text{s}^{-1}$)		$2.11 \pm 0.01 \times 10^7$	$1.28 \pm 0.03 \times 10^7$
k_{off} (s^{-1})		0.0572 ± 0.0003	0.35 ± 0.01
K_i (nM)		2.71	27.05

compound **1** is thus a consequence of its slow binding rate at low concentrations, rather than of enzyme isomerization.

Crystal Structure of huBChE in a Complex with Compound 1. The complex structure of compound (+)-**1** with huBChE was solved at 2.7 Å resolution (Supporting Information, Table S2) from crystals soaked for 1 h in a mother liquor solution supplemented with 100 μM of the compound. With respect to the native structure (PDB code 1P0M),²⁸ no noticeable rearrangement was observed upon binding of compound **1** (Figure 6A).

Examination of the complex structure reveals the molecular basis of the high affinity binding of (+)-**1** to huBChE (Figure 6B). A strong cation– π interaction is observed between the positively charged nitrogen of the piperidine moiety and Tyr332 side chain, while the naphthalene moiety fully occupies the acyl-binding pocket where it T-stacks to the side chain Trp231 (π – π interaction). That this pocket is comparatively smaller in AChE likely explain why compound **1** displays low affinity for the later. In addition, the carbon atoms of the piperidine ring stack between the side chains of Phe329 and Tyr332 and the 1*H*-indene ring lays over the backbone atoms of residues Ile69 and Asp70, thereby stabilizing the molecule at the entrance of the active site gorge. Of note, the methoxyethyl group points toward the catalytic residues Ser198 and His438 (distances between closest non-hydrogen atoms: 5.4 and 4.3 Å, respectively), but does not directly interact with any of them, offering several opportunities for structural modifications of compound **1** to improve its potency (i.e., modification of the chain to catch the polar interaction with the catalytic residues). As both *R* and *S* enantiomers of **1** provided a perfect fit to the

electron density maps, (+)-**1** was assigned to the *R*-enantiomer on the basis of a possible cation– π interaction between the positively charged nitrogen of the piperidine moiety and the side chain of Tyr332 (Figure 7). Of note, a similar structure was

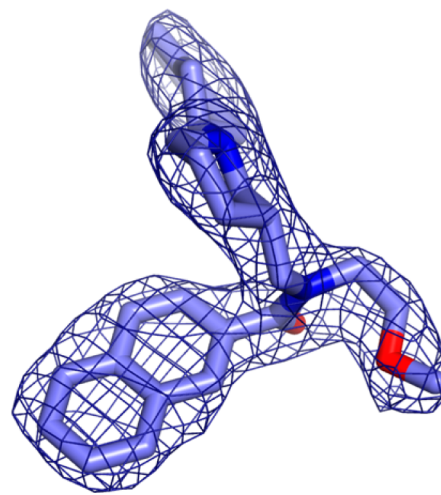


Figure 7. $2mF_o - DF_c$ electron density map (blue mesh, contoured at 1σ) of *R* enantiomer of compound **1** (purple sticks) bound in the active site of huBChE.

obtained when huBChE crystals were soaked into a racemic mixture of (\pm)-**1**, although at a lower resolution (3.2 Å; data not shown). A comparison of the crystal structure pose and the docked pose of compound **1** is discussed in Supporting Information, Figures S5 and S6.

Aggregation and Cell-Based Assays. Senile plaques are extracellular deposits of $A\beta$ found in the gray matter of the AD patient's brains, and they are considered as one of the hallmarks of the disease.^{60,61} The formation of extracellular senile plaques is a multistep process that involves: (i) *in vivo* production of $A\beta$ peptides by sequential proteolytic cleavage of the amyloid precursor protein by the β - and γ -secretases³ and (ii) abnormal aggregation of soluble $A\beta$ monomers into insoluble and

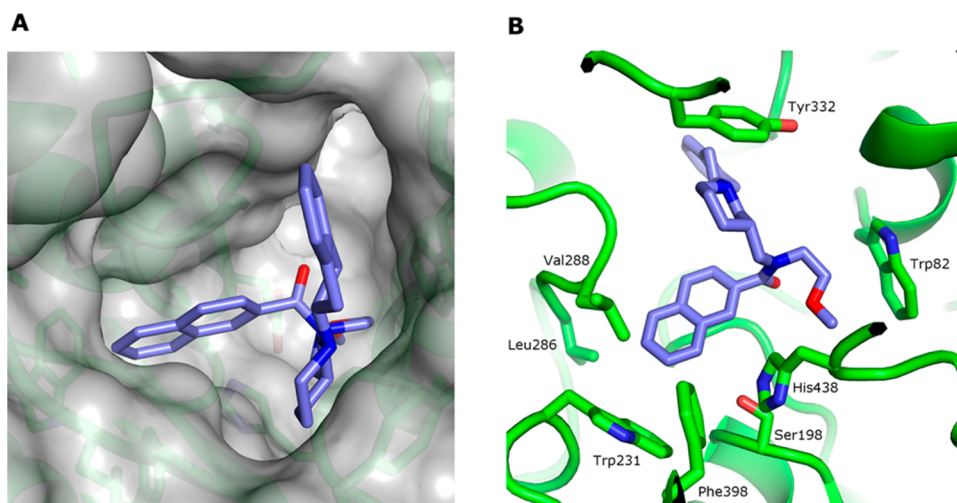


Figure 6. 2.7 Å resolution crystal structure of compound (+)-**1** bound to huBChE (PDB code 4TPK) (A) View from the top of the catalytic pocket, showing compound **1** as purple sticks, bound to the surface of huBChE (in gray). The protein is shown as a cartoon, and the key residues in the catalytic pocket are shown as sticks. (B) Close-up view of compound **1** as purple sticks bound in the acyl-binding pocket of huBChE (green). Residues important for the binding of compound **1** are shown as sticks, as are the catalytic residues (Ser198 and His438).

neurotoxic amyloid fibrils.^{2,58} Although numerous small and large molecules have been studied with the intention to block the expression or cleavage of the $A\beta$ peptides,^{62,63} all such strategies have failed to produce any effective cure for AD to date. As neurotoxicity in AD is primarily associated with the formation and accumulation of $A\beta$ species (mainly $A\beta_{1-42}$), targeting the $A\beta$ self-induced aggregation represents an emerging approach for the discovery of novel neuroprotective agents. Furthermore, combining the antiaggregation properties and BChE inhibition in one single molecule might lead to an anti-AD agent that is effective in the early and late stages of AD.

Several compounds that include indanone, benzoxazole, or benzothiazole moieties have already been shown to have the affinity toward $A\beta_{1-42}$ and also to prevent its aggregation and the formation of fibrils.⁶⁴⁻⁶⁶ Benzothiazole-containing compound **8** was tested for its antiaggregation properties using the ThT fluorescence assay. As the 1*H*-indene moiety is structurally related to the above-mentioned substituents, the possibility of having similar effects was also checked for compound (\pm)-**1**. The procedure for determination of self-induced aggregation was optimized for use with the lowest amount of $A\beta_{1-42}$ that still gave accurate and reproducible results. At 2 μM $A\beta_{1-42}$ solution, the fluorescence reached a plateau within 8 h and remained almost unchanged (within statistic error) between 8 and 48 h of incubation, which is in agreement with the already published kinetics of $A\beta_{1-42}$ self-induced aggregation.⁶⁷ Table 1 summarizes the $A\beta_{1-42}$ self-induced aggregation activity of the novel BChE inhibitors. Compound (\pm)-**1** was tested at 10 μM , where it showed significant $A\beta_{1-42}$ -antiaggregation effects, with 61.7% inhibition. Because of these promising in vitro data for compound **1**, it was further evaluated in cell-based assays. As the pure enantiomers of compound **1** showed nearly identical $A\beta$ -antiaggregation activities, all of the cell-based assays were performed using the racemate.

First, the cytotoxicity profile was assessed using the human neuroblastoma SH-SY5Y cell line and the MTS assay. Compound (\pm)-**1** at 10 μM was completely noncytotoxic (Supporting Information, Figure S4). Next, to determine whether compound (\pm)-**1** can protect neuronal cells from toxic $A\beta$ -species, cell-viability experiments were conducted. To compare neuronal death induced by $A\beta_{1-42}$ in the absence and presence of various concentrations of compound (\pm)-**1**, the MTS assay was performed. As shown in Figure 8a, incubation of SH-SY5Y cells with 5 μM $A\beta_{1-42}$ caused significant toxicity; the cell-death was approximately 35% higher than in the control. A clear dose–response neuroprotective effect was observed when the cells were incubated with $A\beta_{1-42}$ in the presence of compound (\pm)-**1**. Interestingly, at 10 μM , compound (\pm)-**1** completely protected the human neuronal SH-SY5Y cells from $A\beta_{1-42}$ peptide toxicity. Neuroprotective effects were further confirmed by performing a LDH release assay (Figure 8b). Briefly, incubation of the SH-SY5Y cells with 5 μM $A\beta_{1-42}$ led to significant increases in LDH release compared to the control. Again, in the presence of compound (\pm)-**1**, dose–response inhibition of LDH release was observed. The results from the LDH release assay are thus in excellent agreement with those from the MTS assay.

Thus, **1** displays in vitro inhibition of $A\beta_{1-42}$ self-induced aggregation and neuroprotective effect on SH-SY5Y cells against $A\beta_{1-42}$ toxicity that put it forward as a promising hit compound. Further optimization is yet needed to suitably balance antiaggregating and anti-BChE activities.

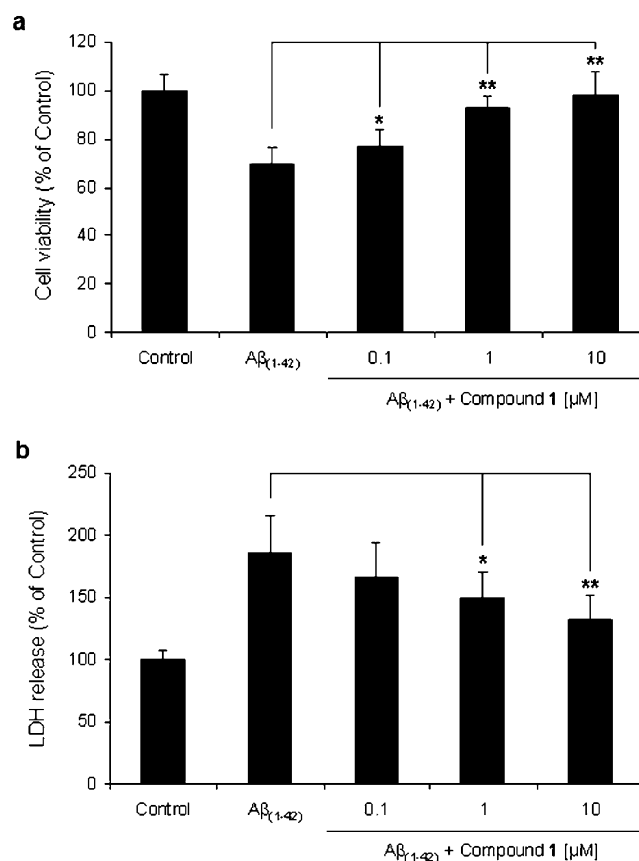


Figure 8. Neuroprotective effects of compound (\pm)-**1** on $A\beta_{1-42}$ -induced cytotoxicity in SH-SY5Y cells. (a) Viability of the SH-SY5Y cells after 48 h with $A\beta_{1-42}$ (5 μM) in the absence and presence of compound (\pm)-**1** at the indicated concentrations, as determined using the MTS assay. The control group (0.1% DMSO) was considered as 100% cell viability, and the assays were carried out in quadruplicate. Data are means \pm SD of at least three independent experiments. (b) Cytotoxicity for the SH-SY5Y cells after exposure to $A\beta_{1-42}$ (5 μM) in the absence and presence of the indicated concentrations of compound **1**, according to the LDH release assay, with the assays carried out in quadruplicate. Data are means \pm SD of two independent experiments. *, $P < 0.05$; **, $P < 0.01$.

CONCLUSIONS

We have described here the application of a hierarchical structure-based virtual screening protocol to the identification of novel inhibitors of huBChE. Using simple tools, the ZINC drug-like library was narrowed down to a much smaller database of compounds with an amine moiety and predicted favorable properties. These were then used in the docking experiment for the final compound selection. Using this approach, we selected and evaluated 40 compounds in vitro and identified three novel hits against huBChE, the most potent of which was compound (\pm)-**1** (IC_{50} = 21.3 nM). We also developed a synthetic route for the resynthesis of the racemic compound **1** and a method for HPLC resolution into its pure enantiomers. The (+)-**1** isomer has an IC_{50} of 13.4 nM against huBChE. Detailed kinetic experiments revealed slow, tight-binding inhibition and a K_i of 2.7 nM for the more potent (+)-**1** enantiomer. The crystal structure of huBChE in complex with compound (+)-**1** confirmed the binding into the active site and revealed possible sites for optimization. At 10 μM , compound (\pm)-**1** also significantly inhibits $A\beta_{1-42}$ self-induced aggregation into fibrils (by 61.7%). Additionally, a clear dose–response

neuroprotective effect against $A\beta$ toxicity was observed on the SH-SY5Y cell line. Considering the low nanomolar BChE inhibitory potency, the crystal structure of the complex, and the promising data from the neuroblastoma cell line, compound **1** represents a valuable hit compound for the development of novel agents against Alzheimer's disease.

EXPERIMENTAL SECTION

Virtual Screening of the Compound Library. *Computer Hardware.* All of the computations were performed on two workstations. The virtual screening was carried out on a workstation with four eight-core AMD Opteron 6128 Magny-Cours 2.0 GHz processors, and 32 GB RAM, two 1 TB hard drives, and a 256 GB solid-state drive, running 64-bit Scientific Linux, release 6.2. The binding-site preparation was carried out on a workstation with two quad-core Intel Xeon 2.2 GHz processors, and 8 GB RAM, 320 GB and 1000 GB hard drives, and a Nvidia Quadro FX 4800 graphic card, running the current version of 64-bit Arch Linux.

Compound Database Preparation. For the virtual screening, the ZINC drug-like subset with 11.3 million drug-like compounds was used.^{47,48} Prior to the docking, hierarchical filtering of the compound database was performed. The ZINC drug-like subset was first filtered with the help of OBGREP, a command-line tool that is part of Open Babel (2.2.3),⁶⁸ a free, open-source program. OBGREP can read compounds from a variety of common chemical file formats and works in a way similar to the UNIX grep command. It performs a SMARTS search through the databases of chemical structures, and allows the user to specify flexible and efficient substructure search specifications. A SMARTS query was formulated which allowed keeping only compounds containing an amine moiety ($[NX3, NX4+, H3, H2, H1, H0; !\$ (NC=O); !\$ (NS=O); !\$ (NN); !\$ (NC=S); !\$ ([N+](=O)[O-])]$). After processing the ZINC drug-like subset with the OBGREP command, only 4.037 million compounds were kept. In the next step, the FILTER 2.0.2 application was used (OpenEye Scientific Software, Inc., Santa Fe, NM, USA; www.eyesopen.com) to eliminate the known or predicted aggregators (a function developed by Soichet⁶⁹) and the compounds with predicted poor solubility (see Supporting Information for the configuration file). The resulting focused and filtered library consisted of roughly 1.495 million compounds. In the final step, the database was processed with the Omega 2.4.3 software (OpenEye Scientific Software, Inc., Santa Fe, NM, USA; www.eyesopen.com),^{70,71} using the default settings to prepare different conformations of compounds that covered as much conformational space as possible. A database of 1.495 million compounds with an average of 158 conformations per compound was then used for the molecular docking.

Molecular Docking. To generate the model for docking trials, we aligned PDB entries 1POM and 1POI, corresponding to the complex structures of BChE with choline, on one hand, and butyrate and glycerol, on the other, using the PyMOL software. Using FRED RECEPTOR 2.2.5 software (OpenEye Scientific Software, Inc., Santa Fe, NM, USA; www.eyesopen.com), we generated a box of 3039 Å³ covering the choline (Trp82 and Glu197) and acyl binding (Trp231, Leu286, Val 288, and Phe398) pockets, as well as the peripheral site of the enzyme. Excluding the active site gorge residues, the docking volume was thus 915 Å³. Of note, neither the protonation state of the active site residues nor their conformations were modified. In practice, the model used for our docking trials corresponded to PDB entry 1POM stripped of all nonprotein atoms, including choline, waters, and sugars. We then generated a high-quality site shape potential of the docking volume. In the final step, custom constraints were used to restrict the poses considered by the docking software, whereby all poses not in the vicinity of Trp82 and Ser198 were discarded. Finally, all of the 1.495 million compounds were docked into the prepared enzyme active site using the FRED 2.2.5 software and the Chemgauss3 scoring function (OpenEye Scientific Software, Inc., Santa Fe, NM, USA, www.eyesopen.com).^{72–74} The docked compounds were ranked according to their best-scored conformation.

Chemistry. General Information. ¹H NMR and ¹³C NMR were recorded at 400 and 100 MHz, respectively, on a Bruker Avance III NMR spectrophotometer. The chemical shifts (δ) are reported in parts per million (ppm) and are referenced to the deuterated solvent used. The coupling constants (J) are reported in Hz, and the splitting patterns are indicated as s (singlet), bs (broad singlet), d (doublet), bd (broad doublet), dd (doublet of doublets), t (triplet), bt (broad triplet), dt (doublet of triplets), q (quartet), and m (multiplet). Infrared (IR) spectra were recorded on a PerkinElmer FT-IR system Spectrum BX. Mass spectra were recorded on a VG-Analytical AutoSpec Q Micromass mass spectrometer. Melting points were determined on a Leica hot-stage microscope and are uncorrected. Evaporation of the solvents was performed at reduced pressure. Reagents and solvents were purchased from Acros Organics, Alfa Aesar, Euriso-Top, Fluka, Merck, Sigma-Aldrich, and TCI Europe and were used without further purification unless otherwise stated. Flash column chromatography was performed on silica gel 60 for column chromatography (particle size, 230–400 mesh). Analytical thin-layer chromatography was performed on Merck silica gel 60 F254 aluminum sheets (0.20 mm), with visualization using ultraviolet light and/or visualization reagents. Analytical reversed-phase HPLC, analytical reversed-phase chiral HPLC, and semipreparative reversed-phase chiral HPLC were performed on an Agilent 1100 LC modular system equipped with an autosampler, a quaternary pump system, a photodiode array detector, a thermostated column compartment, a fraction collector compartment, and a ChemStation data system. The detector was set to 210.16, 254.16, and 280.16 nm. The column used for the methods A and D analytical reversed-phase HPLC was a Zorbax Eclipse Plus C18 analytical column (150 mm \times 4.6 mm, 5 μ m; Agilent). An HPLC Guard cartridge system was used, as a Security Guard cartridge C18 COPS (octadecyl; 4.0 mm \times 3.0 mm ID; Phenomenex). The column used for the methods B and E analytical reversed-phase chiral HPLC was a Kromasil 3-CelluCoat RP column (150 mm \times 4.6 mm). The column used for the method C semipreparative reversed-phase chiral HPLC was a Kromasil 5-CelluCoat RP column (250 mm \times 10 mm). A Guard Cartridge was used with this column, as a Kromasil 5-CelluCoat RP (10–21.2 mm). The HPLC columns were thermostated at 25 °C.

Method A. The sample solution (10 μ L; 0.1 mg/mL in acetonitrile [MeCN]) was injected and eluted at a flow rate of 1 mL/min, using a linear gradient of mobile phase A (MeCN) and mobile phase B (aqueous phosphate buffer: 20 mM, pH 8.00). The gradient for method A (for mobile phase A) was: 0–15 min, 30%–70%; 15–20 min, 70%; 20–25 min, 70%–30%.

Method B. The sample solution of (\pm)-**1** (10 μ L; 0.2 mg/mL in MeCN) was injected and eluted over 30 min at a flow rate of 0.8 mL/min, using aqueous sodium borate buffer (20 mM, pH 9.00) containing 49% MeCN.

Method C. The sample solution of (\pm)-**1** (100 μ L; 10 mg/mL in MeCN) was injected and eluted over 42 min at a flow rate of 5 mL/min, using aqueous sodium borate buffer (20 mM, pH 9.00) containing 49% MeCN.

Method D. The sample solution (10 μ L; 0.1 mg/mL in MeCN) was injected and eluted at a flow rate of 1 mL/min, using a linear gradient of mobile phase A (0.1% trifluoroacetic acid [TFA]; [v/v] in MeCN) and mobile phase B (0.1% aqueous TFA [v/v]). The gradient for method D (for mobile phase A) was: 0–16 min, 10%–90%; 16–19 min, 90%; 19–20 min, 90%–10%.

Method E. The sample solution of (\pm)-**1** (20 μ L; 0.5 mg/mL in MeCN) was injected and eluted over 30 min at a flow rate of 0.6 mL/min, using aqueous sodium borate buffer (20 mM, pH 9.00) containing 50% MeCN.

*Synthesis of (\pm)-tert-Butyl 2-Methoxyethyl(piperidin-3-ylmethyl)-carbamate [(\pm)-**4**].* To a 250 mL round-bottomed flask with a stirring bar, (\pm)-**3** (4.137 g, 11.412 mmol, 1.0 equiv) and MeOH (160 mL) were added at room temperature. The resulting solution was stirred and agitated with a stream of argon for 30 min. Pd(OH)₂ on carbon (20 wt %) (0.828g, 20% mass of (\pm)-**3**) was added, followed by cyclohexene (11.571 mL, 114.122 mmol, 10.0 equiv). The resulting suspension was refluxed under an atmosphere of argon for 17 h then

filtered through a pad of Celite and evaporated to produce 3.015 g of crude amine (\pm)-4 as a colorless oil (97% yield). This product was used in the next step without further purification. $R_f = 0.44$ ($\text{CH}_2\text{Cl}_2/\text{MeOH}/\text{Et}_3\text{N}$; 20:2:1, v/v/v). $^1\text{H NMR}$ (400 MHz, CDCl_3): $\delta = 1.00\text{--}1.14$ (1 H, m), 1.37–1.49 (10 H, m), 1.60–1.80 (5 H, m), 2.25–2.37 (1 H, m), 2.51–2.58 (1 H, m), 2.95–3.00 (2 H, m), 3.13–3.25 (1 H, m), 3.28–3.38 (5 H, m), 3.44–3.52 (2 H, m). HRMS (ESI⁺): m/z calcd for $\text{C}_{14}\text{H}_{29}\text{N}_2\text{O}_3$ 273.2178; found 273.2174.

Synthesis of 1*H*-Inden-2(3*H*)-one (5). A mixture of pyridinium chlorochromate (6.426 g, 29.811 mmol, 2.0 equiv) and silica gel (6.426 g, 70–230 mesh) was ground to a fine powder using a pestle and mortar. The light-orange mixture was added to a 250 mL round-bottomed flask with a stirring bar, and CH_2Cl_2 (80 mL) was added. The resulting orange suspension was stirred at room temperature, and 2-indanol (2.000 g, 14.905 mmol, 1.0 equiv) was added in small portions. After 130 min, the resulting dark-brown suspension was diluted with Et_2O (60 mL) and filtered under suction through a Büchner funnel layered with silica gel (70–230 mesh) and Celite. The dark-brown precipitate was washed thoroughly with Et_2O (3 × 20 mL). The combined filtrates were evaporated. The residue was purified by flash column chromatography using Et_2O /petroleum ether (1:4, v/v) as the eluent, to produce 1.302 g of ketone 5 as a slightly golden oil that solidified into a slightly yellow solid after cooling (66% yield). $R_f = 0.46$ (Et_2O /petroleum ether, 1:1, v/v); mp 51–53 °C (lit.²⁵ mp 52–54 °C). $^1\text{H NMR}$ (400 MHz, CDCl_3): $\delta = 3.58$ (4 H, s), 7.21–7.32 (4 H, m).

Synthesis of (\pm)-tert-Butyl (1-(2,3-Dihydro-1*H*-inden-2-yl)-piperidin-3-yl)methyl(2-methoxyethyl)carbamate [(\pm)-6]. To a 100 mL round-bottomed flask with a stirring bar, (\pm)-4 (1.094 g, 4.016 mmol, 1.0 equiv) and 1,2-dichloroethane (50 mL) were added at room temperature. The resulting solution was stirred and agitated with a stream of argon for 15 min. $\text{NaBH}(\text{OAc})_3$ (1.596 g, 7.530 mmol, 1.875 equiv), 5 (0.531 g, 4.018 mmol, 1.0 equiv), and AcOH (0.230 mL, 4.018 mmol, 1.0 equiv) were added, and the resulting suspension was stirred under an atmosphere of argon for 72 h. The reaction mixture was opened to the air and quenched with saturated aqueous NaHCO_3 solution (50 mL). The mixture was transferred into a 250 mL separating funnel, and CH_2Cl_2 (20 mL) was added. The separating funnel was shaken vigorously, and the organic phase was separated, dried over anhydrous Na_2SO_4 , and evaporated. The residue was purified by flash column chromatography using $\text{CH}_2\text{Cl}_2/\text{MeOH}$ (30:1, v/v) as the eluent to produce 1.292 g of amine (\pm)-6 as a slightly golden oil (83% yield). $R_f = 0.50$ ($\text{CH}_2\text{Cl}_2/\text{MeOH}$, 10:1, v/v); $[\alpha]_D^{23}$ 0.0 (c 0.300, CHCl_3). IR (NaCl): 2930, 2359, 1692, 1463, 1414, 1365, 1170, 1117, 1010, 867, 743, 526 cm^{-1} . $^1\text{H NMR}$ (400 MHz, $\text{DMSO}-d_6$, 60 °C): $\delta = 0.90\text{--}0.99$ (1 H, m), 1.40 (9 H, s), 1.56–1.67 (2 H, m), 1.77–1.88 (2 H, m), 2.01–2.07 (1 H, m), 2.73–2.81 (4 H, m), 2.95–3.02 (2 H, m), 3.10 (2 H, d, $J = 6.90$ Hz), 3.14–3.15 (3 H, m), 3.25 (3 H, s), 3.28–3.31 (1 H, m), 3.41–3.44 (2 H, m), 7.07–7.12 (2 H, m), 7.15–7.19 (2 H, m). $^{13}\text{C NMR}$ (100 MHz, $\text{DMSO}-d_6$, 60 °C): $\delta = 24.08, 27.70, 27.85, 35.92, 36.02, 46.29, 51.18, 54.95, 57.67, 66.13, 78.09, 123.76, 125.78, 141.04, 141.10, 154.52$. HRMS (ESI⁺): m/z calcd for $\text{C}_{23}\text{H}_{37}\text{N}_2\text{O}_3$ 389.2804; found 389.2798. HPLC purity, 99% at 210.16 nm (method A, $t_R = 19.61$ min).

Synthesis of (\pm)-*N*-((1-(2,3-Dihydro-1*H*-inden-2-yl)piperidin-3-yl)methyl)-2-methoxyethanamine [(\pm)-7]. To a 100 mL round-bottomed flask equipped with a stirring bar, (\pm)-6 (1.203 g, 3.096 mmol, 1.0 equiv) and CH_2Cl_2 (50 mL) were added at room temperature. The resulting solution was stirred and TFA (2.371 mL, 30.960 mmol, 10.0 equiv) was added dropwise. After 22 h, the reaction mixture was evaporated. The residue was coevaporated with CH_2Cl_2 (2 × 40 mL), followed by *n*-hexane (2 × 50 mL). Et_2O (50 mL) was added to the oily residue, and the flask was placed in an ultrasonic bath for 15 min. During this time, the oily residue transformed into a white solid. The flask was removed from the ultrasonic bath, and the precipitate was allowed to settle to the bottom of the flask. The supernatant was removed, Et_2O (30 mL) was added, and the flask was placed back in the ultrasonic bath for 1 min. The flask was removed from the ultrasonic bath, and the precipitate was allowed to settle to the bottom of the flask. The supernatant was removed, Et_2O (30 mL)

was added again, and this procedure was repeated two more times. After the final supernatant was removed, the solid residue was dried at reduced pressure. Water (15 mL) and a stirring bar were added, and the resulting solution was cooled to 0 °C and adjusted to pH 12 with 1 M aqueous NaOH. The mixture was transferred into a 50 mL separating funnel, extracted with CH_2Cl_2 (2 × 30 mL), dried over anhydrous Na_2SO_4 , and evaporated to produce 0.750 g of crude secondary amine (\pm)-7 as a slightly brown oil (84% yield). This product was used in the next step without further purification. $R_f = 0.38$ ($\text{CH}_2\text{Cl}_2/\text{MeOH}/\text{Et}_3\text{N}$, 40:4:1, v/v/v). $^1\text{H NMR}$ (400 MHz, CDCl_3): $\delta = 0.90\text{--}1.00$ (1 H, m), 1.57–1.83 (6 H, m), 1.94–2.01 (1 H, m), 2.55 (2 H, d, $J = 6.40$ Hz), 2.77 (2 H, t, $J = 5.15$ Hz), 2.89–2.98 (3 H, m), 3.03–3.21 (4 H, m), 3.36 (3 H, s), 3.50 (2 H, t, $J = 5.14$ Hz), 7.11–7.19 (4 H, m). HRMS (ESI⁺): m/z calcd for $\text{C}_{18}\text{H}_{29}\text{N}_2\text{O}$ 289.2280; found 289.2273.

Synthesis of (\pm)-*N*-((1-(2,3-Dihydro-1*H*-inden-2-yl)piperidin-3-yl)methyl)-*N*-(2-methoxyethyl)-2-naphthamide [(\pm)-1]. To a 50 mL round-bottomed flask with a stirring bar, 2-naphthoic acid (0.423g, 2.457 mmol, 1.0 equiv) and CH_2Cl_2 (20 mL) were added at room temperature. The resulting suspension was stirred, and Et_3N (0.685 mL, 4.914 mmol, 2.0 equiv) was added dropwise. The solution was stirred for 5 min before *O*-(benzotriazol-1-yl)-*N,N,N',N'*-tetramethyluronium tetrafluoroborate (TBTU; 0.789 g, 2.457 mmol, 1.0 equiv) was added in small portions. After 30 min, a solution of (\pm)-7 (0.709 g, 2.458 mmol, 1.0 equiv) in CH_2Cl_2 (10 mL) was added dropwise, and the reaction mixture was stirred for 19 h. The solvent was evaporated, the residue dissolved in EtOAc (60 mL), transferred into a 250 mL separating funnel, and extracted with H_2O (2 × 50 mL) and then aqueous saturated NaHCO_3 solution (50 mL), and dried over anhydrous Na_2SO_4 and evaporated. The residue was purified by flash column chromatography using $\text{CH}_2\text{Cl}_2/\text{MeOH}$ (20:1, v/v) as the eluent and then precipitated from Et_2O to produce 0.391 g of amide (\pm)-1 as a white solid (36% yield). $R_f = 0.48$ ($\text{CH}_2\text{Cl}_2/\text{MeOH}$, 10:1, v/v); mp 54–57 °C $[\alpha]_D^{23}$ 0.0 (c 0.285, CHCl_3). IR (KBr): 3546, 3209, 2929, 2144, 1622, 1487, 1418, 1301, 1112, 827, 748, 482 cm^{-1} . $^1\text{H NMR}$ (400 MHz, $\text{DMSO}-d_6$, 60 °C): $\delta = 0.93$ (1 H, bs), 1.44–1.46 (1 H, m), 1.63 (2 H, bs), 1.98 (2 H, bs), 2.67–2.79 (4 H, m), 2.95–3.00 (2 H, m), 3.15 (3 H, s), 3.23 (2 H, bs), 3.44 (6 H, bd), 7.08–7.13 (2 H, m), 7.16–7.21 (2 H, m), 7.40–7.43 (1 H, m), 7.54–7.60 (2 H, m), 7.88 (1 H, s), 7.94–7.98 (3 H, m). $^{13}\text{C NMR}$ (100 MHz, $\text{DMSO}-d_6$, 60 °C): $\delta = 24.00, 27.85, 34.24, 35.84, 35.90, 51.01, 54.68, 57.75, 65.98, 69.28, 123.75, 123.80, 124.06, 125.44, 125.79, 126.25, 126.43, 127.27, 127.53, 127.79, 131.93, 132.47, 134.25, 141.14, 141.16, 170.76$. HRMS (ESI⁺): m/z calcd for $\text{C}_{29}\text{H}_{35}\text{N}_2\text{O}_2$ 443.2699; found 443.2696. HPLC purity, 99% at 254.16 nm (method A, $t_R = 18.11$ min).

Separation of (+)-1 and (–)-1 by Semipreparative Reverse-Phase Chiral HPLC. The resolution of (\pm)-1 was accomplished by 65 runs of method C. Eluates corresponding to the two chromatographic peaks were pooled and evaporated to about 5 mL and then transferred to a 50 mL separating funnel. Water (6 mL) and aqueous saturated NaHCO_3 solution (6 mL) were added and extracted with CH_2Cl_2 (25 mL). The organic phase was dried over anhydrous Na_2SO_4 and evaporated to produce 30.6 mg of the first-eluted enantiomer as a colorless oil and 31.7 mg of the second-eluted enantiomer as a colorless oil. Analytical reversed-phase chiral HPLC analysis (method B, $\lambda = 254.16$ nm) of the first-eluted enantiomer gave an enantiomeric excess (ee) of 100%, whereas the ee of the second-eluted enantiomer was 98%. The specific rotation of the first-eluted enantiomer was $[\alpha]_D^{23} -23.82$ (c 0.250, CHCl_3), while the specific rotation of the second-eluted enantiomer was $[\alpha]_D^{23} +24.52$ (c 0.260, CHCl_3). The analytical reversed-phase chiral HPLC retention times were (method B, $\lambda = 254.16$ nm): (–)-1, 21.09 min; (+)-1, 22.36 min.

In Vitro Enzyme Inhibition Studies. Inhibitory Activity against the Cholinesterases. The inhibitory activity of the compounds was determined using the method of Ellman.⁵¹ 5,5'-Dithiobis(2-nitrobenzoic acid) (Ellman's reagent, DTNB), butyrylthiocholine (BTC), and acetylthiocholine (ATC) iodides were purchased from Sigma-Aldrich (Steinheim, Germany). The lyophilized powders of murine (m)AChE and recombinant huBChE were dissolved in 10 mM MES buffer (pH 6.5) to give an enzyme stock solution of 4 mg/mL.

The enzyme solutions were prepared by dilution of the concentrated stock in a phosphate-buffered solution (0.1 M, pH 8.0). The reactions were carried out in a final volume of 300 μL of 0.1 M phosphate-buffered solution, pH 8.0, containing 333 μM DTNB, 5×10^{-4} M BTC/ATC, and 1×10^{-9} M or 5×10^{-11} M huBChE or mAChE, respectively. The reactions were started by addition of the substrate at room temperature. The final content of organic solvent (dimethyl sulfoxide; DMSO) was always 1%. The formation of the yellow 5-thio-2-nitrobenzoate anion as a result of the reaction of DTNB with the thiocholines was monitored for 1 min as change in absorbance at 412 nm, using a 96-well microplate reader (Synergy H4, BioTek Instruments, Inc., USA). To determine the blank value (b), phosphate-buffered solution replaced the enzyme solution. The initial velocity (v_0) was calculated from the slope of the linear trend obtained, with each measurement carried out in triplicate. For the first inhibitory screening, stock solutions of the test compounds (1 mM) were prepared in DMSO. The compounds were added to each well at a final concentration of 10 μM . The reactions were started by the addition of the substrate to the enzyme and inhibitor that had been preincubated for 300 s to allow complete equilibration of the enzyme–inhibitor complexes. All of the solutions were carefully monitored to detect possible precipitation or agglomeration of the compounds. The initial velocity in the presence of the test compound (v_i) was calculated. The inhibitory potency was expressed as the residual activity ($\text{RA} = v_i - b / v_0 - b$). For the IC_{50} measurements, eight different concentrations of each compound were used to obtain enzyme activities of between 5% and 90%. The IC_{50} values were obtained by plotting the residual enzyme activities against the applied inhibitor concentrations, with the experimental data fitted to the equation: $Y = \text{bottom} + (\text{top} - \text{bottom}) / (1 + 10^{(\text{LogIC}_{50} - X) \times \text{HillSlope}})$, where X is the logarithm of the inhibitor concentration, and Y is the residual activity. For the fitting procedure, the Gnuplot software and an in-house python script were used.

HuBChE Inhibition Kinetic Studies. To determine the mode of action of huBChE inhibition by (\pm)-1 and its pure enantiomers, we followed the time-course of yellow color formation on a Biologic SFM-2000 stopped flow apparatus at 25 $^{\circ}\text{C}$. The two buffer solutions were prepared as one that contained the substrate BTC, the reagent DTNB, and the test compound 1 (either as a racemate or as each pure enantiomer), and the other that contained the huBChE. The buffer solutions were injected into a mixing chamber using syringes. The resulting solution contained 45.3 μM BTC, 1 mM DTNB, 4.2 nM huBChE, 50 nM test compound, and 0.007 M DMSO (i.e., 0.05%). The absorbance was followed at 412 nm immediately and until the change reached zero. The progress curves obtained were analyzed simultaneously, with the ENZO application,⁷⁶ which can derive and numerically solve a system of differential equations, and fit their coefficients. Several reaction mechanisms were tested. The simplest one for the reproduction of the progress curves in the absence and presence of (\pm)-1, (+)-1 and (–)-1 was chosen, and the corresponding inhibition constants were determined. The results file can be accessed by loading the ENZO project ID 140429302, selecting the “Set Parameters” tab, and pressing “Start”.

Crystallization, Data Collection, and Processing. huBChE from insect cells was concentrated to 6 mg/mL in 10 mM Tris, pH 7.4 and crystallized as previously described.³⁵ Briefly, crystals were grown at room-temperature using the hanging-drop vapor diffusion method. The mother liquor solution was 0.2 M ammonium acetate and 14% polyethylene glycol 3500. Crystals were soaked for 1 h in a solution of the mother liquor complemented with compound (+)-1 at 100 μM concentration. Prior to data collection, crystals were cryoprotected by a short soak in a mother liquor solution complemented with 18% glycerol before being flash-cooled directly in a N_2 gas stream at 100 K. Data were collected at beamline ID14-EH4 of the European Synchrotron Radiation Facility (Grenoble, France) using a wavelength of 0.873 \AA . Data were indexed and integrated using XDS,⁷⁷ and were scaled and merged with XSCALE and XDSCONV (Supporting Information, Table S2). The structure was solved by the molecular replacement method using PHASER,⁷⁸ using as a search model the huBChE model (PDB code 1POM), from which all ligands and sugars

were removed. Reciprocal-space refinement was performed using Phenix;⁷⁹ briefly, initial rigid-body refinement and simulated annealing were followed by cycles of energy minimization and grouped isotropic temperature factor refinement. Local NCS restraints between the two huBChE monomers in the asymmetric unit were applied during refinement procedure, as well as the use of a reference model as a prior structural knowledge.⁸⁰ The model refinement was interspersed with sessions of model rebuilding using the program Coot.⁸¹ The ligand topology was generated with the PRODRG server.⁸² Coordinates and structure factors have been deposited in the Protein Data Bank under accession code 4TPK.

Inhibition of Amyloid $\beta_{(1-42)}$ Peptide Self-Induced Aggregation. To investigate the effect of the test compounds on the self-aggregation of $A\beta_{1-42}$, a thioflavin T-based fluorometric assay was performed.⁸³ Recombinant human 1,1,1,3,3,3-hexafluoro-2-propanol-pretreated $A\beta_{1-42}$ peptide (Merck Millipore, Darmstadt, Germany) was dissolved in DMSO as a 100 μM stock solution. Prior to the incubations, the $A\beta_{1-42}$ peptide stock solution was diluted in 150 mM HEPES buffer (pH 7.4) containing 150 mM NaCl to give a concentration of 10 μM . Then 20 μL of $A\beta_{1-42}$ was mixed with 10 μL of the test compounds (100 μM stock in HEPES; 10 μM final concentration), added to the corresponding wells in black-walled 96-well plates, and immediately diluted with 70 μL of thioflavin T solution (ThT) (14.3 μM stock solution in HEPES; 10 μM final concentration) to the final volume of 100 μL (2 μM final $A\beta_{1-42}$ concentration). Each sample was prepared in quadruplicate, and the DMSO was always at 3%. Aggregation was initiated by placing the sealed 96-well plate at 37 $^{\circ}\text{C}$ in a plate reader (Synergy H4). To quantify amyloid fibril formation, the ThT fluorescence was measured through the bottom of the plate every 90 s at an excitation wavelength of 440 nm and emission wavelength of 490 nm, with the medium continuously shaking between measurements. The ThT emission of the $A\beta_{1-42}$ began to rise after 1 h, reached a plateau after 8 h, and remained almost unchanged for an additional 16 h of incubation. The fluorescence intensities at the plateau in the absence and presence of the test compounds were averaged, and the average fluorescence of the corresponding wells at $t = 0$ h was subtracted. The eq $(1 - F_i/F_0) \times 100\%$ was used to quantify the inhibition of $A\beta_{1-42}$ self-induced aggregation, where F_i is the increase in fluorescence of $A\beta_{1-42}$ treated with the test compounds and F_0 is the increase in fluorescence of $A\beta_{1-42}$ alone.

Cell Culture and Treatments. Human neuroblastoma SH-SY5Y cells were purchased from American Type Culture Collection (CRL-2266, Manassas, VA, USA). The cells were grown in Dulbecco's Modified Eagle's Medium (Sigma, St. Louis, MO, USA) supplemented with 10% fetal bovine serum (HyClone, Logan, UT, USA), 2 mM L-glutamine, 50 U/mL penicillin, and 50 $\mu\text{g}/\text{mL}$ streptomycin (Sigma, St. Louis, MO, USA) in a humidified atmosphere of 95% air and 5% CO_2 at 37 $^{\circ}\text{C}$ and grown to 80% confluence. Prior to cell treatment, the complete medium was replaced with reduced-serum medium (2% fetal bovine serum). The compounds were prepared as stock solutions of 10 mM in DMSO and were used at concentrations of 0.1–100 μM . For the cytotoxic stimuli, $A\beta_{1-42}$ was dissolved in DMSO as a 5 mM stock solution, and 6 h before the cell treatment, $A\beta_{1-42}$ was incubated at a final concentration of 5 μM in reduced-serum medium in the absence and presence of the test compounds (0.1–10 μM) at 37 $^{\circ}\text{C}$, to induce $A\beta_{1-42}$ aggregation.

Cell Viability Assay. The SH-SY5Y cells were seeded in 96-well plates ($2 \times 10^4/\text{well}$) and assessed using the MTS (3-(4,5-dimethylthiazol-2-yl)-5-(3-carboxymethoxyphenyl)-2-(4-sulfophenyl)-2H-tetrazolium, inner salt) assay for their response to the test compound treatments or to preaggregated $A\beta_{1-42}$ in the presence of the test compounds. The cells were treated as described above, and the cell viabilities were assessed after 48 h, using the CellTiter 96 Aqueous one solution cell proliferation assay (Promega, Madison, WI, USA), according to the manufacturer instructions. The absorbance was measured using an automatic microplate reader (Tecan Safire2, Switzerland) at a wavelength of 492 nm. The data are presented as percentages of the control (0.1% DMSO).

Lactate Dehydrogenase Assay. Cell toxicity was measured by determining the activity of the lactate dehydrogenase (LDH) released into the medium when the cell membranes were damaged. The SH-SY5Y cells were seeded into 24-well culture plates (1×10^5 /well). After the cells were treated with $A\beta_{1-42}$ in the absence and presence of the test compounds for 48 h, the supernatants and cell lysates were collected and the amount of LDH released was determined following the specifications of the CytoTox-ONE homogeneous membrane integrity assay (Promega, Madison, WI, USA). Fluorescence was measured using an automatic microplate reader (Tecan Safire2) at an excitation wavelength of 560 nm and an emission wavelength of 590 nm. The LDH release is expressed as the percentages of the total LDH activity, as normalized to the LDH release of the control (0.1% DMSO).

■ ASSOCIATED CONTENT

■ Supporting Information

Results of the in silico screen for the 40 top-ranked structures from the ZINC database, FILTER configuration file, hit purity data, dose–response curves with IC_{50} determinations, reactivation after (\pm)-1-huBChE preincubation, chromatograms of chiral HPLC resolution of (\pm)-1, cytotoxicity profile of the virtual screening hits, X-ray crystallography data collection statistics, the comparison of the docked and crystal structure pose of compound 1, and AChE molecular docking studies. This material is available free of charge via the Internet at <http://pubs.acs.org>

Accession Codes

Atomic coordinates and structure factors for the crystal structure of huBChE in complex with compound 1 can be accessed using PDB code 4TPK.

■ AUTHOR INFORMATION

Corresponding Authors

*For S.G.: phone, +386-1-4769500; fax, +386-1-4258031; E-mail, stanislav.gobec@ffa.uni-lj.si.

*For J.P.C.: phone, +33457428515; fax, +33476501890; E-mail, Jacques-Philippe.Colletier@ibs.fr.

Present Address

∇ BioMed X GmbH, Im Neuenheimer Feld 583, 69120 Heidelberg, Germany.

Notes

The authors declare no competing financial interest.

■ ACKNOWLEDGMENTS

This work was supported by the Slovenian Research Agency. We thank OpenEye Scientific Software, Santa Fe, NM, for free academic licenses of their software and Institut Francais for financial support. We thank Florian Nachon, Xavier Brazoletto, Marielle Vandhammer, and Marie Trosvalet for providing us with lyophilized murine AChE and human BChE as well as for continuous and fruitful discussions. Financial support by the France-Alzheimer Foundation and the Agence Nationale de la Recherche (ANR) is gratefully acknowledged. We also thank Dr. Chris Berrie for critical reading of the manuscript.

■ ABBREVIATIONS USED

AChE, acetylcholinesterase; AD, Alzheimer's disease; $A\beta$, amyloid- β ; ACh, acetylcholine; ATC, acetylthiocholine iodide; BChE, butyrylcholinesterase; BTC, butyrylthiocholine iodide; ChE, cholinesterase; DMSO, dimethyl sulfoxide; DTNB, dithiobis(2-nitrobenzoic acid) (Ellman's reagent); ee, enantiomeric excess; PDB, Protein Data Bank; ThT, thioflavin T

■ REFERENCES

- (1) Wimo, A.; Jönsson, L.; Bond, J.; Prince, M.; Winblad, B. The Worldwide Economic Impact of Dementia 2010. *Alzheimer's Dementia* **2013**, *9*, 1–11.
- (2) Glabe, C. C. Amyloid Accumulation and Pathogenesis of Alzheimer's Disease: Significance of Monomeric, Oligomeric and Fibrillar $A\beta$. In *Alzheimer's Disease; Subcellular Biochemistry*; Harris, J. R.; Fahrenholz, F., Eds.; Springer: New York, 2005; pp 167–177.
- (3) Sinha, S.; Lieberburg, I. Cellular Mechanisms of B-Amyloid Production and Secretion. *Proc. Natl. Acad. Sci. U. S. A.* **1999**, *96*, 11049–11053.
- (4) Gella, A.; Durany, N. Oxidative Stress in Alzheimer Disease. *Cell Adhes. Migr.* **2009**, *3*, 88–93.
- (5) Scarpini, E.; Schelterns, P.; Feldman, H. Treatment of Alzheimer's Disease; Current Status and New Perspectives. *Lancet Neurol.* **2003**, *2*, 539–547.
- (6) Perry, E. K.; Tomlinson, B. E.; Blessed, G.; Bergmann, K.; Gibson, P. H.; Perry, R. H. Correlation of Cholinergic Abnormalities with Senile Plaques and Mental Test Scores in Senile Dementia. *Br. Med. J.* **1978**, *2*, 1457–1459.
- (7) Tago, H.; Maeda, T.; McGeer, P. L.; Kimura, H. Butyrylcholinesterase-Rich Neurons in Rat Brain Demonstrated by a Sensitive Histochemical Method. *J. Comp. Neurol.* **1992**, *325*, 301–312.
- (8) Kawakami, Y.; Inoue, A.; Kawai, T.; Wakita, M.; Sugimoto, H.; Hopfinger, A. J. The Rationale for E2020 as a Potent Acetylcholinesterase Inhibitor. *Bioorg. Med. Chem.* **1996**, *4*, 1429–1446.
- (9) Kryger, G.; Silman, I.; Sussman, J. L. Structure of Acetylcholinesterase Complexed with E2020 (Aricept): Implications for the Design of New Anti-Alzheimer Drugs. *Structure* **1999**, *7*, 297–307.
- (10) Bar-On, P.; Millard, C. B.; Harel, M.; Dvir, H.; Enz, A.; Sussman, J. L.; Silman, I. Kinetic and Structural Studies on the Interaction of Cholinesterases with the Anti-Alzheimer Drug Rivastigmine. *Biochemistry (Moscow)* **2002**, *41*, 3555–3564.
- (11) Greenblatt, H. M.; Kryger, G.; Lewis, T.; Silman, I.; Sussman, J. L. Structure of Acetylcholinesterase Complexed with (–)-Galanthamine at 2.3 Å Resolution. *FEBS Lett.* **1999**, *463*, 321–326.
- (12) Mesulam, M.-M.; Guillozet, A.; Shaw, P.; Levey, A.; Duysen, E.; Lockridge, O. Acetylcholinesterase Knockouts Establish Central Cholinergic Pathways and Can Use Butyrylcholinesterase to Hydrolyze Acetylcholine. *Neuroscience* **2002**, *110*, 627–639.
- (13) Li, B.; Duysen, E. G.; Carlson, M.; Lockridge, O. The Butyrylcholinesterase Knockout Mouse as a Model for Human Butyrylcholinesterase Deficiency. *J. Pharmacol. Exp. Ther.* **2008**, *324*, 1146–1154.
- (14) Holmes, C.; Ballard, C.; Lehmann, D.; Smith, A. D.; Beaumont, H.; Day, I. N.; Khan, M. N.; Lovestone, S.; McCulley, M.; Morris, C. M.; Munoz, D. G.; O'Brien, K.; Russ, C.; Ser, T. D.; Warden, D. Rate of Progression of Cognitive Decline in Alzheimer's Disease: Effect of Butyrylcholinesterase K Gene Variation. *J. Neurol. Neurosurg. Psychiatry* **2005**, *76*, 640–643.
- (15) Hartmann, J.; Kiewert, C.; Duysen, E. G.; Lockridge, O.; Greig, N. H.; Klein, J. Excessive Hippocampal Acetylcholine Levels in Acetylcholinesterase-Deficient Mice Are Moderated by Butyrylcholinesterase Activity. *J. Neurochem.* **2007**, *100*, 1421–1429.
- (16) Greig, N. H.; Yu, Q.; Brossi, A.; Soncrant, T. T.; Hausman, M. Highly Selective Butyrylcholinesterase Inhibitors for the Treatment and Diagnosis of Alzheimer's Disease and Dementias. U.S. Patent 20020094999, July 18, 2002.
- (17) Greig, N. H.; Utsuki, T.; Ingram, D. K.; Wang, Y.; Pepeu, G.; Scali, C.; Yu, Q.-S.; Mamczarz, J.; Holloway, H. W.; Giordano, T.; Chen, D.; Furukawa, K.; Sambamurti, K.; Brossi, A.; Lahiri, D. K. Selective Butyrylcholinesterase Inhibition Elevates Brain Acetylcholine, Augments Learning and Lowers Alzheimer B-Amyloid Peptide in Rodent. *Proc. Natl. Acad. Sci. U. S. A.* **2005**, *102*, 17213–17218.
- (18) Furukawa-Hibi, Y.; Alkam, T.; Nitta, A.; Matsuyama, A.; Mizoguchi, H.; Suzuki, K.; Moussaoui, S.; Yu, Q.-S.; Greig, N. H.; Nagai, T.; Yamada, K. Butyrylcholinesterase Inhibitors Ameliorate

Cognitive Dysfunction Induced by Amyloid-B Peptide in Mice. *Behav. Brain Res.* **2011**, *225*, 222–229.

(19) Giacobini, E. Cholinesterase Inhibitors: New Roles and Therapeutic Alternatives. *J. Ital. Pharmacol. Soc.* **2004**, *50*, 433–440.

(20) McGleenon, B. M.; Dynan, K. B.; Passmore, A. P. Acetylcholinesterase Inhibitors in Alzheimer's Disease. *Br. J. Clin. Pharmacol.* **1999**, *48*, 471–480.

(21) Ballard, C.; Greig, N.; Guillozet-Bongaarts, A.; Enz, A.; Darvesh, S. Cholinesterases: Roles in the Brain During Health and Disease. *Curr. Alzheimer Res.* **2005**, *2*, 307–318.

(22) Kamal, M. A.; Qu, X.; Yu, Q.; Tweedie, D.; Holloway, H. W.; Li, Y.; Tan, Y.; Greig, N. H. Tetrahydrofurobenzofuran Cymserine, a Potent Butyrylcholinesterase Inhibitor and Experimental Alzheimer Drug Candidate, Enzyme Kinetic Analysis. *J. Neural Transm.* **2008**, *115*, 889–898.

(23) Carolan, C. G.; Dillon, G. P.; Khan, D.; Ryder, S. A.; Gaynor, J. M.; Reidy, S.; Marquez, J. F.; Jones, M.; Holland, V.; Gilmer, J. F.; Isosorbide-2-Benzyl Carbamate-5-Salicylate, A Peripheral Anionic Site Binding Subnanomolar Selective Butyrylcholinesterase Inhibitor. *J. Med. Chem.* **2010**, *53*, 1190–1199.

(24) Minarini, A.; Milelli, A.; Tumiatti, V.; Rosini, M.; Simoni, E.; Bolognesi, M. L.; Andrisano, V.; Bartolini, M.; Motori, E.; Angeloni, C.; Hrelia, S. Cystamine–Tacrine Dimer: A New Multi-Target-Directed Ligand as Potential Therapeutic Agent for Alzheimer's Disease Treatment. *Neuropharmacology* **2011**, *62*, 997–1003.

(25) Galdeano, C.; Viayna, E.; Sola, I.; Formosa, X.; Camps, P.; Badia, A.; Clos, M. V.; Relat, J.; Ratia, M.; Bartolini, M.; Mancini, F.; Andrisano, V.; Salmona, M.; Minguillón, C.; González-Muñoz, G. C.; Rodríguez-Franco, M. L.; Bidon-Chanal, A.; Luque, F. J.; Muñoz-Torrero, D. Huprine–Tacrine Heterodimers as Anti-Amyloidogenic Compounds of Potential Interest against Alzheimer's and Prion Diseases. *J. Med. Chem.* **2012**, *55*, 661–669.

(26) Fernández-Bachiller, M. I.; Pérez, C.; González-Muñoz, G. C.; Conde, S.; López, M. G.; Villarroya, M.; García, A. G.; Rodríguez-Franco, M. I. Novel Tacrine–8-Hydroxyquinoline Hybrids as Multifunctional Agents for the Treatment of Alzheimer's Disease, with Neuroprotective, Cholinergic, Antioxidant, and Copper-Complexing Properties. *J. Med. Chem.* **2010**, *53*, 4927–4937.

(27) Lange, J. H. M.; Coolen, H. K. A. C.; van der Neut, M. A. W.; Borst, A. J. M.; Stork, B.; Verveer, P. C.; Kruse, C. G. Design, Synthesis, Biological Properties, and Molecular Modeling Investigations of Novel Tacrine Derivatives with a Combination of Acetylcholinesterase Inhibition and Cannabinoid CB1 Receptor Antagonism. *J. Med. Chem.* **2010**, *53*, 1338–1346.

(28) Nicolet, Y.; Lockridge, O.; Masson, P.; Fontecilla-Camps, J. C.; Nachon, F. Crystal Structure of Human Butyrylcholinesterase and of Its Complexes with Substrate and Products. *J. Biol. Chem.* **2003**, *278*, 41141–41147.

(29) Cheung, J.; Rudolph, M. J.; Burshteyn, F.; Cassidy, M. S.; Gary, E. N.; Love, J.; Franklin, M. C.; Height, J. J. Structures of Human Acetylcholinesterase in Complex with Pharmacologically Important Ligands. *J. Med. Chem.* **2012**, *55*, 10282–10286.

(30) Dvir, H.; Silman, I.; Harel, M.; Rosenberry, T. L.; Sussman, J. L. Acetylcholinesterase: From 3D Structure to Function. *Chem.–Biol. Interact.* **2010**, *187*, 10–22.

(31) Raveh, L.; Grauer, E.; Grunwald, J.; Cohen, E.; Ashani, Y. The Stoichiometry of Protection against Soman and VX Toxicity in Monkeys Pretreated with Human Butyrylcholinesterase. *Toxicol. Appl. Pharmacol.* **1997**, *145*, 43–53.

(32) Masson, P.; Nachon, F.; Broomfield, C. A.; Lenz, D. E.; Verdier, L.; Schopfer, L. M.; Lockridge, O. A Collaborative Endeavor to Design Cholinesterase-Based Catalytic Scavengers against Toxic Organophosphorus Esters. *Chem.–Biol. Interact.* **2008**, *175*, 273–280.

(33) Brazzilotto, X.; Wandhammer, M.; Ronco, C.; Trovaslet, M.; Jean, L.; Lockridge, O.; Renard, P.-Y.; Nachon, F. Human Butyrylcholinesterase Produced in Insect Cells: Huprine-Based Affinity Purification and Crystal Structure. *FEBS J.* **2012**, *279*, 2905–2916.

(34) Hamulakova, S.; Janovec, L.; Hrabínova, M.; Spilovska, K.; Korabecny, J.; Kristian, P.; Kuca, K.; Imrich, J. Synthesis and Biological Evaluation of Novel Tacrine Derivatives and Tacrine–Coumarin Hybrids as Cholinesterase Inhibitors. *J. Med. Chem.* **2014**, *57*, 7073–7084.

(35) Tasso, B.; Catto, M.; Nicolotti, O.; Novelli, F.; Tonelli, M.; Giangreco, I.; Pisani, L.; Sparatore, A.; Boido, V.; Carotti, A.; Sparatore, F. Quinolizidinyl Derivatives of Bi- and Tricyclic Systems as Potent Inhibitors of Acetyl- and Butyrylcholinesterase with Potential in Alzheimer's Disease. *Eur. J. Med. Chem.* **2011**, *46*, 2170–2184.

(36) Cappelli, A.; Gallelli, A.; Manini, M.; Anzini, M.; Mennuni, L.; Makovec, F.; Menziani, M. C.; Alcaro, S.; Ortuso, F.; Vomero, S. Further Studies on the Interaction of the 5-Hydroxytryptamine₃ (5-HT₃) Receptor with Arylpiperazine Ligands. Development of a New 5-HT₃ Receptor Ligand Showing Potent Acetylcholinesterase Inhibitory Properties. *J. Med. Chem.* **2005**, *48*, 3564–3575.

(37) Shoichet, B. K. Virtual Screening of Chemical Libraries. *Nature* **2004**, *432*, 862–865.

(38) Schneider, G. Virtual Screening: An Endless Staircase? *Nature Rev. Drug Discovery* **2010**, *9*, 273–276.

(39) Reddy, A. S.; Pati, S. P.; Kumar, P. P.; Pradeep, H. N.; Sastry, G. N. Virtual Screening in Drug Discovery—A Computational Perspective. *Curr. Protein Pept. Sci.* **2007**, *8*, 329–351.

(40) Ripphausen, P.; Nisius, B.; Peltason, L.; Bajorath, J. Quo Vadis, Virtual Screening? A Comprehensive Survey of Prospective Applications. *J. Med. Chem.* **2010**, *53*, 8461–8467.

(41) Cheng, T.; Li, Q.; Zhou, Z.; Wang, Y.; Bryant, S. H. Structure-Based Virtual Screening for Drug Discovery: A Problem-Centric Review. *AAPS J.* **2012**, *14*, 133–141.

(42) Cummings, M. D.; Gibbs, A. C.; DesJarlais, R. L. Processing of Small Molecule Databases for Automated Docking. *Curr. Top. Med. Chem. (Sharjah United Arab Emirates)* **2007**, *3*, 107–113.

(43) Felder, C. E.; Botti, S. A.; Lifson, S.; Silman, I.; Sussman, J. L. External and Internal Electrostatic Potentials of Cholinesterase Models. *J. Mol. Graphics Modell.* **1997**, *15* (318–327), 335–337.

(44) Nolte, H. J.; Rosenberry, T. L.; Neumann, E. Effective Charge on Acetylcholinesterase Active Sites Determined from the Ionic Strength Dependence of Association Rate Constants with Cationic Ligands. *Biochemistry (Moscow)* **1980**, *19*, 3705–3711.

(45) Bourne, Y.; Radić, Z.; Sulzenbacher, G.; Kim, E.; Taylor, P.; Marchot, P. Substrate and Product Trafficking through the Active Center Gorge of Acetylcholinesterase Analyzed by Crystallography and Equilibrium Binding. *J. Biol. Chem.* **2006**, *281*, 29256–29267.

(46) Bartolucci, C.; Stojan, J.; Yu, Q.; Greig, N. H.; Lamba, D. Kinetics of *Torpedo Californica* Acetylcholinesterase Inhibition by Bisnorcymserine and Crystal Structure of the Complex with Its Leaving Group. *Biochem. J.* **2012**, *444*, 269–277.

(47) Irwin, J. J.; Sterling, T.; Mysinger, M. M.; Bolstad, E. S.; Coleman, R. G. ZINC: A Free Tool to Discover Chemistry for Biology. *J. Chem. Inf. Model.* **2012**, *52*, 1757–1768.

(48) Lipinski, C. A. Drug-like Properties and the Causes of Poor Solubility and Poor Permeability. *J. Pharmacol. Toxicol. Methods* **2000**, *44*, 235–249.

(49) Kellenberger, E.; Rodrigo, J.; Muller, P.; Rognan, D. Comparative Evaluation of Eight Docking Tools for Docking and Virtual Screening Accuracy. *Proteins: Struct., Funct., Bioinform.* **2004**, *57*, 225–242.

(50) Schomburg, K.; Ehrlich, H.-C.; Stierand, K.; Rarey, M. From Structure Diagrams to Visual Chemical Patterns. *J. Chem. Inf. Model.* **2010**, *50*, 1529–1535.

(51) Ellman, G. L.; Courtney, K. D.; Andres, V., Jr.; Featherstone, R. M. A New and Rapid Colorimetric Determination of Acetylcholinesterase Activity. *Biochem. Pharmacol.* **1961**, *7*, 88–95.

(52) Kořák, U.; Brus, B.; Gobec, S. Straightforward Synthesis of Orthogonally Protected Piperidin-3-ylmethanamine and Piperidin-4-ylmethanamine Derivatives. *Tetrahedron Lett.* **2014**, *55*, 2037–2039.

- (53) Macleod, C.; Martinez-Teipel, B. I.; Barker, W. M.; Dolle, R. E. Annulation of Primary Amines to Piperazines and Diazaspirocycles Utilizing A-Methyl Benzyl Resin. *J. Comb. Chem.* **2006**, *8*, 132–140.
- (54) Luzzio, F. A.; Fitch, R. W.; Moore, W. J.; Mudd, K. J. A Facile Oxidation of Alcohols Using Pyridinium Chlorochromate/Silica Gel. *J. Chem. Educ.* **1999**, *76*, 974.
- (55) Abdel-Magid, A. F.; Carson, K. G.; Harris, B. D.; Maryanoff, C. A.; Shah, R. D. Reductive Amination of Aldehydes and Ketones with Sodium Triacetoxyborohydride. Studies on Direct and Indirect Reductive Amination Procedures I. *J. Org. Chem.* **1996**, *61*, 3849–3862.
- (56) Balalaie, S.; Mahdidoust, M.; Eshaghi-Najafabadi, R. 2-(1H-Benzotriazole-1-yl)-1,1,3,3-tetramethyluronium Tetrafluoroborate as an Efficient Coupling Reagent for the Amidation and Phenylhydrazination of Carboxylic Acids at Room Temperature. *J. Iran. Chem. Soc.* **2007**, *4*, 364–369.
- (57) Šinko, G.; Kovarik, Z.; Reiner, E.; Simeon-Rudolf, V.; Stojan, J. Mechanism of Stereoselective Interaction between Butyrylcholinesterase and Ethopropazine Enantiomers. *Biochimie* **2011**, *93*, 1797–1807.
- (58) Cha, S. Tight-Binding Inhibitors—I: Kinetic Behavior. *Biochem. Pharmacol.* **1975**, *24*, 2177–2185.
- (59) Copeland, R. A. Tight Binding Inhibition. In *Evaluation of Enzyme Inhibitors in Drug Discovery*; John Wiley & Sons, Inc.: New York, 2013; pp 245–285.
- (60) Cras, P.; Kawai, M.; Lowery, D.; Gonzalez-DeWhitt, P.; Greenberg, B.; Perry, G. Senile Plaque Neurites in Alzheimer Disease Accumulate Amyloid Precursor Protein. *Proc. Natl. Acad. Sci. U. S. A.* **1991**, *88*, 7552–7556.
- (61) Hardy, J.; Selkoe, D. J. The Amyloid Hypothesis of Alzheimer's Disease: Progress and Problems on the Road to Therapeutics. *Science* **2002**, *297*, 353–356.
- (62) Dash, P. K.; Moore, A. N.; Orsi, S. A. Blockade of Gamma-Secretase Activity within the Hippocampus Enhances Long-Term Memory. *Biochem. Biophys. Res. Commun.* **2005**, *338*, 777–782.
- (63) Asai, M.; Hattori, C.; Iwata, N.; Saido, T. C.; Sasagawa, N.; Szabó, B.; Hashimoto, Y.; Maruyama, K.; Tanuma, S.; Kiso, Y.; Ishiura, S. The Novel Beta-Secretase Inhibitor KMI-429 Reduces Amyloid Beta Peptide Production in Amyloid Precursor Protein Transgenic and Wild-Type Mice. *J. Neurochem.* **2006**, *96*, 533–540.
- (64) Huang, L.; Lu, C.; Sun, Y.; Mao, F.; Luo, Z.; Su, T.; Jiang, H.; Shan, W.; Li, X. Multitarget-Directed Benzylideneindanone Derivatives: Anti-B-Amyloid (A β) Aggregation, Antioxidant, Metal Chelation, and Monoamine Oxidase B (MAO-B) Inhibition Properties against Alzheimer's Disease. *J. Med. Chem.* **2012**, *55*, 8483–8492.
- (65) Cui, M.; Ono, M.; Kimura, H.; Ueda, M.; Nakamoto, Y.; Togashi, K.; Okamoto, Y.; Ihara, M.; Takahashi, R.; Liu, B.; Saji, H. Novel 18F-Labeled Benzoxazole Derivatives as Potential Positron Emission Tomography Probes for Imaging of Cerebral B-Amyloid Plaques in Alzheimer's Disease. *J. Med. Chem.* **2012**, *55*, 9136–9145.
- (66) Wu, C.; Pike, V. W.; Wang, Y. Amyloid Imaging: From Benchtop to Bedside. In *In Vivo Cellular and Molecular Imaging: Current Topics in Developmental Biology*; Ahrens, E. T., Ed.; Academic Press: New York, 2005; Vol. 70, pp 171–213.
- (67) Cohen, S. I. A.; Linse, S.; Luheshi, L. M.; Hellstrand, E.; White, D. A.; Rajah, L.; Otzen, D. E.; Vendruscolo, M.; Dobson, C. M.; Knowles, T. P. J. Proliferation of Amyloid- β 42 Aggregates Occurs through a Secondary Nucleation Mechanism. *Proc. Natl. Acad. Sci. U. S. A.* **2013**, *110*, 9758–9763.
- (68) O'Boyle, N. M.; Banck, M.; James, C. A.; Morley, C.; Vandermeersch, T.; Hutchison, G. R. Open Babel: An Open Chemical Toolbox. *J. Cheminformatics* **2011**, *3*, 33.
- (69) Shoichet, B. K. Interpreting Steep Dose–Response Curves in Early Inhibitor Discovery. *J. Med. Chem.* **2006**, *49*, 7274–7277.
- (70) Hawkins, P. C. D.; Nicholls, A. Conformer Generation with OMEGA: Learning from the Data Set and the Analysis of Failures. *J. Chem. Inf. Model.* **2012**, *52*, 2919–2936.
- (71) Hawkins, P. C. D.; Skillman, A. G.; Warren, G. L.; Ellingson, B. A.; Stahl, M. T. Conformer Generation with OMEGA: Algorithm and Validation Using High Quality Structures from the Protein Databank and Cambridge Structural Database. *J. Chem. Inf. Model.* **2010**, *50*, 572–584.
- (72) McGann, M. FRED Pose Prediction and Virtual Screening Accuracy. *J. Chem. Inf. Model.* **2011**, *51*, 578–596.
- (73) McGaughey, G. B.; Sheridan, R. P.; Bayly, C. I.; Culberson, J. C.; Kreatsoulas, C.; Lindsley, S.; Maiorov, V.; Truchon, J.-F.; Cornell, W. D. Comparison of Topological, Shape, and Docking Methods in Virtual Screening. *J. Chem. Inf. Model.* **2007**, *47*, 1504–1519.
- (74) McGann, M. R.; Almond, H. R.; Nicholls, A.; Grant, J. A.; Brown, F. K. Gaussian Docking Functions. *Biopolymers* **2003**, *68*, 76–90.
- (75) Barlas, H.; Kotzias, D.; Parlar, H. Photoreaktionen von Stickstoffdioxid Mit Indan in Lösung. *Chemosphere* **1985**, *14*, 1231–1238.
- (76) Bevc, S.; Konc, J.; Stojan, J.; Hodošek, M.; Penca, M.; Praprotnik, M.; Janežič, D. ENZO: A Web Tool for Derivation and Evaluation of Kinetic Models of Enzyme Catalyzed Reactions. *PLoS One* **2011**, *6*, e22265.
- (77) Kabsch, W. XDS. *Acta Crystallogr., Sect. D: Biol. Crystallogr.* **2010**, *66*, 125–132.
- (78) McCoy, A. J.; Grosse-Kunstleve, R. W.; Adams, P. D.; Winn, M. D.; Storoni, L. C.; Read, R. J. Phaser Crystallographic Software. *J. Appl. Crystallogr.* **2007**, *40*, 658–674.
- (79) Adams, P. D.; Afonine, P. V.; Bunkóczi, G.; Chen, V. B.; Davis, I. W.; Echols, N.; Headd, J. J.; Hung, L.-W.; Kapral, G. J.; Grosse-Kunstleve, R. W.; McCoy, A. J.; Moriarty, N. W.; Oeffner, R.; Read, R. J.; Richardson, D. C.; Richardson, J. S.; Terwilliger, T. C.; Zwart, P. H. PHENIX: A Comprehensive Python-Based System for Macromolecular Structure Solution. *Acta Crystallogr., Sect. D: Biol. Crystallogr.* **2010**, *66*, 213–221.
- (80) Headd, J. J.; Echols, N.; Afonine, P. V.; Grosse-Kunstleve, R. W.; Chen, V. B.; Moriarty, N. W.; Richardson, D. C.; Richardson, J. S.; Adams, P. D. Use of Knowledge-Based Restraints in *phenix.refine* to Improve Macromolecular Refinement at Low Resolution. *Acta Crystallogr., Sect. D: Biol. Crystallogr.* **2012**, *68*, 381–390.
- (81) Emsley, P.; Lohkamp, B.; Scott, W. G.; Cowtan, K. Features and Development of *Coot*. *Acta Crystallogr., Sect. D: Biol. Crystallogr.* **2010**, *66*, 486–501.
- (82) Schüttelkopf, A. W.; van Aalten, D. M. F. PRODRG: A Tool for High-Throughput Crystallography of Protein–Ligand Complexes. *Acta Crystallogr., Sect. D: Biol. Crystallogr.* **2004**, *60*, 1355–1363.
- (83) LeVine, H. Thioflavine T Interaction with Synthetic Alzheimer's Disease Beta-Amyloid Peptides: Detection of Amyloid Aggregation in Solution. *Protein Sci.* **1993**, *2*, 404–410.